Neutral Silicon-Vacancy Center in Diamond: Spin Polarization and Lifetimes

B. L. Green,[1,*] S. Mottishaw,[1] B. G. Breeze,[1] A. M. Edmonds,[2] U. F. S. D'Haenens-Johansson,[3] M. W. Doherty,[4] S. D. Williams,[2] D. J. Twitchen,[2] and M. E. Newton[1,†]

[1]*Department of Physics, University of Warwick, Coventry CV4 7AL, United Kingdom*
[2]*Element Six Limited, Global Innovation Centre, Fermi Avenue OX11 0QR, United Kingdom*
[3]*Gemological Institute of America, 50 W 47th Street, New York, New York 10036, USA*
[4]*Laser Physics Centre, Research School of Physics and Engineering, Australian National University, Australian Capital Territory 0200, Australia*

(Received 31 May 2017; published 31 August 2017)

We demonstrate optical spin polarization of the neutrally charged silicon-vacancy defect in diamond (SiV^0), an $S = 1$ defect which emits with a zero-phonon line at 946 nm. The spin polarization is found to be most efficient under resonant excitation, but nonzero at below-resonant energies. We measure an ensemble spin coherence time $T_2 > 100$ μs at low-temperature, and a spin relaxation limit of $T_1 > 25$ s. Optical spin-state initialization around 946 nm allows independent initialization of SiV^0 and NV^- within the same optically addressed volume, and SiV^0 emits within the telecoms down-conversion band to 1550 nm: when combined with its high Debye-Waller factor, our initial results suggest that SiV^0 is a promising candidate for a long-range quantum communication technology.

DOI: 10.1103/PhysRevLett.119.096402

Point defects in diamond have attracted considerable interest owing to their application for quantum information processing, communication, and metrology. The most-studied defect, the negatively charged nitrogen-vacancy (NV^-) center, possesses efficient optical spin polarization and spin-state dependent fluorescence, enabling its exploitation as an ultrasensitive nanoscale magnetic field sensor [1–3]. However, the zero phonon line (ZPL) of NV^- accounts for only a few percent of its total emission [4], leading to low efficiency in coherent photonic applications. The negatively charged silicon-vacancy (SiV^-) center has also received significant interest as its high Debye-Waller factor (≈0.8 [5]) makes it an attractive candidate for long-range quantum computation and communication. However, the exceptional optical properties of SiV^- are not matched by its spin properties, where a large spin-orbit coupling in the ground state enables phonon-assisted spin-state depopulation, resulting in spin-lattice relaxation-limited coherence lifetimes of 40 ns even at 5 K [6]: efforts are ongoing to overcome this limitation by strain engineering, but currently, liquid helium temperatures and below are required to access and readout SiV^- spin states [7].

The neutrally charged silicon-vacancy (SiV^0) has a ground state electron spin of $S = 1$. Unlike the NV center, where the nitrogen remains covalently bonded to three carbon atoms and the nitrogen-vacancy axis forms a C_{3v} symmetry axis, the silicon atom in SiV adopts a bond-center location, with a D_{3d} axis formed by the $\langle 111 \rangle$ joining the split vacancy [Fig. 1(a)]. SiV^0 has been characterized both by electron paramagnetic resonance (EPR) [8,9] and optical absorption or photoluminescence (PL) [10]. Similar to SiV^-, the neutral charge state also has a high Debye-Waller factor, with the majority of its photons emitted at the primary ZPL at 946 nm (1.31 eV) [Fig. 1(b)]: polarized absorption measurements assign it to a transition between a ${}^3A_{2g}$ ground state (GS) and ${}^3A_{1u}$ excited state (ES) [10,11]. Quenching of PL at low temperature indicates the presence of a shelving state 5 meV below the ES [10]. The zero-field splitting (ZFS) in the GS is $D = +1000$ MHz at 300 K [9]. The ZFS is highly temperature-dependent, being approximately linear in the range 50–150 K with $dD/dT = -337$ kHz K^{-1}, and an average of -202 kHz K^{-1} between 50 and 300 K—these values are significantly higher than for NV^- at -74 kHz K^{-1} [12]. Finally, nonequilibrium populations of the four symmetry-related defect orientations have been observed in grown-in SiV^0 when the diamond crystal is grown on substrates of particular crystallographic orientation [10]. This behavior has been previously observed in NV^- [13,14] and SiV^- [15].

We have studied SiV^0 in two samples grown by chemical vapor deposition: sample A contains 5(2) ppb of SiV^0;

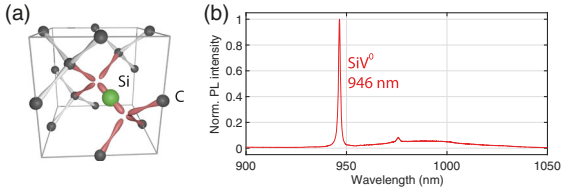

FIG. 1. (a) The structure of the silicon-vacancy defect in the diamond lattice: the silicon adopts a bond-center location, leading to D_{3d} symmetry ($\langle 111 \rangle$ axis) in both the neutral and negative charge states [16]. (b) Photoluminescence spectrum of SiV^0 (zero phonon line at 946 nm) at a temperature of 80 K in sample B. The feature at 976 nm is related to SiV^0 and may indicate local strain [11].

 © 2017 American Physical Society

sample B has 75(8) ppb of SiV^0 (see [17] for details). To investigate the behavior of SiV^0 under optical excitation, we perform both cw and pulsed EPR measurements (Bruker E580 spectrometer) using a dielectric resonator (Bruker ER 4118X-MD5) and cryostat (Oxford Instruments CF935) for variable temperature measurements. Optical excitation from various laser sources is delivered to the sample via a $\phi 1$ mm core fiber held in place with a Rexolite rod [Fig. 2(a)]. For pulsed measurements, the 532 nm laser (CNI MGLIII532) is switched using an acousto-optic modulator. Quantitative EPR measurements are carried out using nonsaturating microwave powers.

Figure 2(b) illustrates the effect of *in situ* continuous optical pumping at 830 nm on the EPR spectrum of SiV^0. The low- and high-field resonances spin polarize into enhanced absorption and emission, respectively, under optical pumping. The ZFS of SiV^0 is known to be positive [9] (i.e., $|m_s\rangle = \pm 1$ are higher in energy than $|m_s\rangle = 0$ at zero magnetic field), and thus, the low- and high-field resonances correspond to the $m_s = 0 \leftrightarrow +1$ and $m_s = 0 \leftrightarrow -1$ transitions. Therefore, the optical pumping is generating enhanced population in the $m_s = 0$ state [Fig. 2, inset]—analogous to the polarization behavior observed in NV^- when excited with a light of wavelength ≤ 637 nm. Qualitatively similar polarization is observed in both samples for excitation at 532 (2.33 eV), 830 (1.49 eV), and 915 nm (1.36 eV) at both 80 and 10 K [17]. Given the high Debye-Waller factor of SiV^0 [Fig. 1(b)], it is surprising that spin polarization is generated over such a wide energy range. Photoconductivity measurements of diamond containing SiV^0 indicate a strong photocurrent at 830 nm [23], and hence, charge effects are expected to be important for excitation at 830 nm and below: the polarization may, therefore, be a result of the capture of a hole (electron) at SiV^- (SiV^+), and not intrinsic to SiV^0. Theoretical studies indicate that green excitation may also excite from deep valence-band states [11].

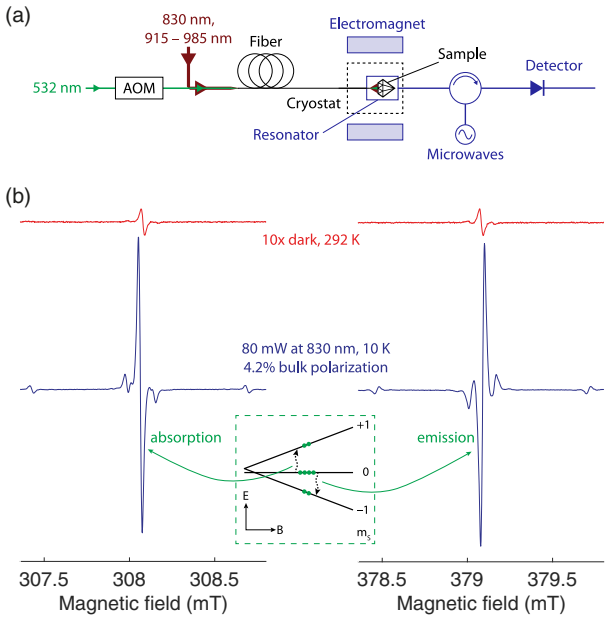

FIG. 2. (a) Schematic of optically pumped EPR measurements. Light from a laser is delivered via optical fiber to the sample mounted into the cryostat. cw measurements performed using lasers at 532, 830, 915 nm and a tuneable 915–985 nm. The 532 nm laser is switched using an acousto-optic modulator (AOM) for pulsed EPR measurements. Components of the EPR spectrometer are in blue. (b) EPR spectra of the $m_s = 0 \leftrightarrow +1$ (left) and $m_s = 0 \leftrightarrow -1$ (right) transitions of SiV^0 in sample A, collected with applied magnetic field B within 2° of $\langle 111 \rangle$. Upper spectra collected at room temperature; lower spectra collected at a sample temperature of 10 K during optical pumping with 80 mW (10.2 W cm^{-2}) at 830 nm. The opposite phase of the low- and high-field lines indicate enhanced absorption and emission, respectively: we achieve a bulk polarization of $\xi = 4.2\%$. Optically pumped spectra have been offset for clarity; magnetic field given for room temperature measurement. Inset: schematic of ground-state energy levels with nominal spin-polarized populations illustrating the origin of enhanced absorption and emission.

We investigate the possibility of an internal spin polarization mechanism by performing a Hahn echo-detected optical frequency-swept measurement: the optical frequency of a widely-tuneable narrow-linewidth laser (TOPTICA CTL 950) is swept over the ZPL, and we detect the resulting EPR enhancement by a two-pulse Hahn echo measurement at each frequency [Fig. 3]. A sharp increase in polarization is observed for resonant excitation at the ZPL (946 nm), confirming a spin-polarization mechanism internal to SiV^0 and unambiguously identifying the 946 nm ZPL with SiV^0. In stark contrast to the behavior of NV^-, polarization is observed even at sub-ZPL energies. Additionally, high-resolution measurements reveal a small ZPL splitting of 0.4 nm (≈134 GHz) (Fig. 3, inset).

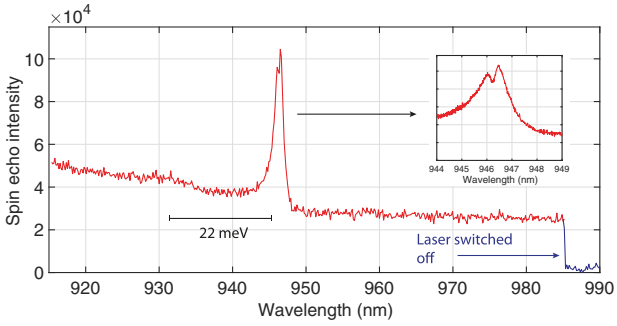

FIG. 3. Spin polarization of sample A measured by a two-pulse Hahn echo while sweeping the incident laser wavelength at an optical power of 9 mW. The spin polarization decreases before reaching a sharp peak at the ZPL wavelength. Above-ZPL excitation continues to generate spin polarization, with a sharp signal decrease observed when the laser is switched off. Inset: high-resolution scans over the ZPL indicate that the ZPL is split by approximately 0.4 nm (≈134 GHz).

The origin of this splitting is unclear: previous optical measurements place the ZPL as a transition between states with no orbital degeneracy ($^3A_{2g} \leftrightarrow {}^3A_{1u}$) [10], and orientational degeneracy is removed by measuring only those defects with their $\langle 111 \rangle$ axis parallel to the magnetic field (see [17] for detail). The effect of strain on a pair of orbital singlets is simply to shift the transition energy [24], and hence, the observed splitting may indicate two populations of defects in distinct strain environments. Alternatively, if the excited state is, in fact, ^3E_u, then Jahn-Teller [25] and spin-orbit effects become significant (excited state spin-orbit splitting in SiV^- is approximately 250 GHz [26]): further investigation is required to determine the microscopic origin of the observed splitting.

We define the degree of spin polarization as $\xi = 100\%$ when all spins are in the $m_s = 0$ state, and $\xi = 0\%$ at thermal equilibrium (see [17] for details of calculation). In both samples, ξ is found to increase from a typical 0.1% at room temperature to approximately 4% at 80 and 10 K for the same excitation [17]. Maximum bulk polarization of 5.2% is observed at 10 K when pumping with 80 mW at 532 nm; maximum per-photon efficiency is found in sample A under resonant ZPL excitation. At all temperatures and wavelengths, the polarization is linear in optical power up to the maximum available at the sample, and therefore, we neglect two-photon processes in our analysis.

The increase of ξ with decreasing temperature may arise from several sources: temperature-dependent effects within the intrinsic spin-polarization mechanism itself can alter the polarization efficiency; and increases in electron longitudinal (spin-lattice) lifetime T_1 can lead to a greater macroscopic buildup of polarization for the same polarization efficiency. The latter was measured directly using the pulse sequence given in Fig. 4(a). The sample was placed in a magnetic field applied within 2° of $\langle 111 \rangle$ at a field strength of 311–316 mT at 292–10 K: the changes in field are a result of the temperature-dependence of both the microwave resonator frequency and the ZFS. The sample was subjected to a polarizing 1.5 ms optical pulse to polarize into the $m_s = 0$ state, and an inverting π pulse of duration 28 ns was applied to the $m_s = 0 \leftrightarrow +1$ transition, transferring polarization into $m_s = +1$. After a variable delay τ, the remaining spin polarization was measured using a Hahn echo detection sequence: this yields an exponentially decaying signal with a single time constant equal to the longitudinal lifetime T_1 [Fig. 4(b)].

The measured T_1 for SiV^0 in sample B are highly temperature dependent [Fig. 4(c)]: unlike NV^-, which retains $T_1 \sim$ ms at room temperature, SiV^0 lifetimes in this sample decrease from approximately 25 s at 15 K to 80 μs at room temperature. EPR linewidth broadening is observed above room temperature [17], and can be used as an indirect measure of T_1 in the limit that $T_2 \leq 2T_1$ [28], indicating $1/T_1 \gtrsim 1$ MHz. The dramatic temperature dependence of T_1 is expected to account for the poor

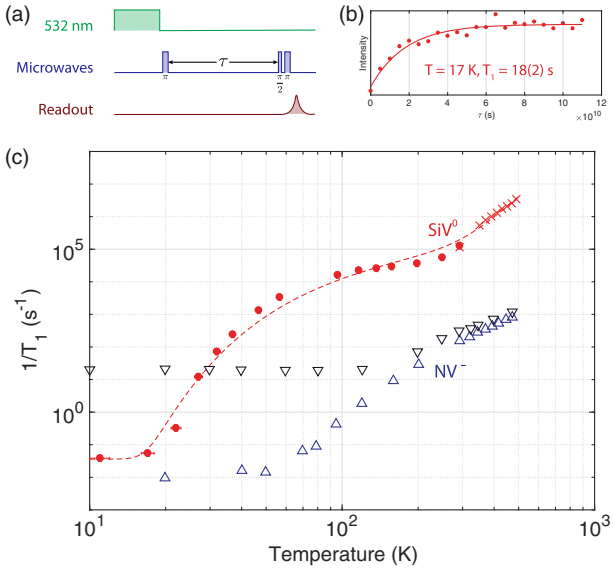

FIG. 4. (a) Pulse sequence used to measure T_1. SiV^0 is spin polarized by optical pumping at 532 nm to increase the signal strength, then an echo-detected inversion-recovery measurement is performed to measure T_1: the inversion pulse is included to enable multistage phase cycling. (b) Echo-detected inversion-recovery measurement at 17 K, yielding a longitudinal spin lifetime of 18(2) s. (c) Temperature dependence of T_1 in SiV^0 (sample B, dots) and NV^- (triangles, two different concentrations—taken from [27]). The SiV^0 spin-lattice relaxation lifetime T_1 depends strongly on temperature in this sample. At low temperatures, $T_1 > 25$ s. Crosses obtained via an indirect measurement of T_1 using linewidth (see [17]); dashed line is a fit to different temperature-dependent relaxation processes (see text).

polarization efficiencies observed at room temperature. Interpretation of spin-lattice lifetimes in solids typically performed in terms of contributions from different phonon processes [29]. Interactions with single phonons (the so-called direct process, $1/T_1 \propto T$) can be neglected, as the spin energies involved at X band, $T = 10\ \mathrm{GHz}/k_B = 0.5$ K are at least an order of magnitude lower than the lowest measurement temperature (11 K). Relaxation via two phonons of different energies—a Raman process—can occur if the energy difference is equal to the spin transition energy, and takes the form $1/T_1 \propto T^n$ where $n \in \{5, 7, 9\}$ depending on the spin levels involved, with $n = 7$ typical for a non-Kramers doublet [29,30]. Finally, the Orbach process describes interaction with an excited spin state at a phonon-accessible energy ΔE above the ground state: the spin is excited by absorption of a phonon of energy $\hbar\Omega_a = \Delta E$ and relaxes to a different ground spin state by emission of a phonon $\hbar\Omega_e \neq \Delta E$. The T_1 data were, therefore, phenomenologically modeled using

$$\frac{1}{T_1} = A_{\mathrm{const}} + A_{\mathrm{Raman}} T^7 + \frac{A_{\mathrm{Orbach}}}{e^{\Delta E/k_B T} - 1}.$$

The fit in Fig. 4(c) was generated using the coefficients $A_{\text{const}} = 0.036\ \text{s}^{-1}$, $A_{\text{Raman}} = 5.0 \times 10^{-13}\ \text{s}^{-1}\,\text{K}^{-1}$, $A_{\text{Orbach}} = 1.5 \times 10^{5}\ \text{s}^{-1}$ and $\Delta E = 22$ meV. The energy $\Delta E = 22$ meV matches the phonon sideband observed in the echo-detected laser-frequency-swept measurement [Fig. 3] and is close to the dominant phonon frequency $\hbar\Omega = 28$ meV estimated from optical absorption measurements [10]: therefore, we conclude that the primary phonon coupling frequency is similar in both the ground and excited states. Multifrequency measurements would enable confirmation of the involved T_1 processes via their magnetic field dependence [29]. Charge transfer effects have not been accounted for and hence the measured $T_{1,\text{effective}}$ is a lower bound at all temperatures.

It is clear that at temperatures above approximately 30 K, SiV^0 T_1 lifetimes are significantly shorter than those of NV^-. At room temperature and below, this is a result of coupling to lower-frequency phonons in the SiV^0 GS (22 meV for SiV^0, and 73 meV for NV^- [27]); above room temperature, the Raman effect dominates in both centers.

The spin coherence time, T_2, is a critical parameter for many applications in sensing and quantum computation [2,31,32]. We measure the T_2 of sample B directly using a Hahn echo-decay sequence ($\pi/2 - \tau - \pi - \tau -$ echo) [30], and find that T_2 changes from 2.0 μs at room temperature to 103 μs at 27 K [Fig. 5]. At both 292 and 96 K, we find $T_2 \approx T_1$, confirming that we are in the limit $T_2 \leq 2T_1$ [28]: at 27 K, $T_2 = 103$ μs is limited by spin-spin interactions rather than $T_1 = 82$ μs. In the lower concentration sample, A, $T_2 = 180$ μs at 27 K. These values are comparable to NV^-, where ensemble measurements reach 630 μs without the use of decoupling sequences [33].

We now consider the source of the spin polarization. In NV^-, the electronic structure relevant to spin polarization is described by the molecular orbitals (MO) $a_1 e$, with the $^3A_2$ GS generated by the configuration $a_1^2 e^2$ [34]. Spin polarization occurs by intersystem crossing (ISC) from the ^3E ES ($a_1^1 e^3$) into a pair of singlets ($^1A_1$, ^1E) arising from the same orbital configuration as the GS [35]. In SiV^0, the $^3A_{2g}$ GS is described by the MO configuration $a_{1g}^2 a_{2u}^2 e_u^4 e_g^2$, which also produces two singlet states $^1A_{1g}$ and ^1E_g. The configuration

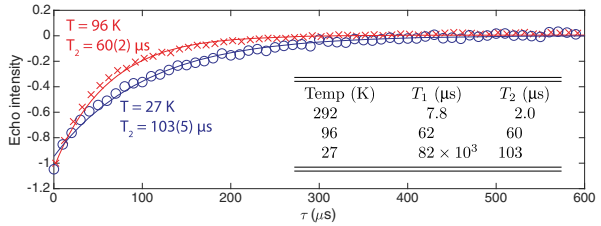

FIG. 5. T_2 decoherence lifetimes measured by echo decay at 96 and 27 K in sample B. Inset: comparison of T_1 and T_2 spin lifetimes. The measured T_2 is effectively limited by $T_2 \leq 2T_1$ at room temperature and 96 K, but has reached a non-T_1-limited value of 103 μs at 27 K.

$a_{1g}^2 a_{2u}^2 e_u^3 e_g^3$ is responsible for the $^3A_{1u}$ ES and additional states $^1A_{1u}$, $^1A_{2u}$, ^1E_u, $^3A_{2u}$, and ^3E_u. The multitude of available states suggests the possibility of spin-orbit (SO) mediated ISC mechanisms, similar to NV^- and other defects in diamond and SiC [36]: any model for SiV^0 must account both for PL quenching at low temperature [10] and spin polarization generated by sub-ZPL excitation. Two of the possible energy level schemes which are consistent with experiment are given in Fig. 6, both based on ISC between singlet and triplet states. Sub-ZPL polarization is generated in Fig. 6(a) by pumping directly into the singlet state, which becomes weakly allowed due to SO effects in the ground state. In Fig. 6(b), no-phonon dipole transitions from the $^3A_{2g}$ GS to the $^3A_{2u}$ ES are forbidden, but transitions into the vibronic sideband would be possible by emission of an A_{2g} phonon. Such an absorption would have no ZPL and the broad band may be difficult to detect. In this model, the spin polarization is generated by ISC from the $^3A_{2u}$ triplet to a singlet (^1E_u), and not from the ES involved in the 946 nm ZPL. Resonant excitation to the $^3A_{1u}$ level would, nevertheless, result in spin polarization via nonradiative transitions from $^3A_{1u}$ to $^3A_{2u}$. In both models, transitions between the singlet states must be dipole forbidden in order for the upper state to be an effective shelving state [10]. Detailed calculation of level

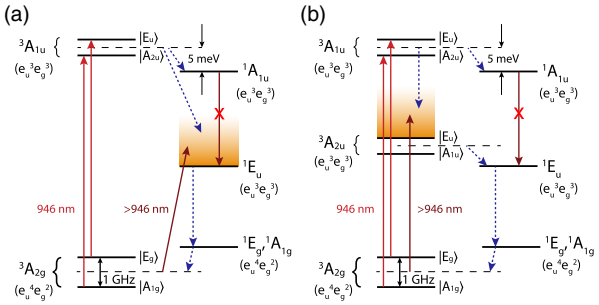

FIG. 6. Possible mechanisms for generation of spin polarization into the GS $m_s = 0$ state based on ISC within SiV^0. Optical transitions are given as solid arrows; non-radiative transitions are dotted. The molecular orbital configuration for each state is given in brackets, spin-orbit (SO) states are given and spin-spin effects have been neglected. (a) Spin polarization occurs by spin-orbit coupling between the ES and a singlet state; below-ZPL polarization is generated by a dipole-allowed transition from the GS to the singlet which becomes weakly allowed due to SO mixing in the GS. (b) Spin polarization is generated by ISC from a third triplet state between the GS and ES. ZPL dipole transitions between the GS and the $^3A_{2u}$ are forbidden, but can be driven into the vibronic sideband by emission of A_{2g} phonons. In both cases, the given singlet characters are examples; however, there can be no dipole transition between singlets in order for the upper singlet to be an effective shelving state, as observed in temperature-dependent PL measurements [10]. In comparison to the well-understood model for NV^- [34], our model must also account for spin polarization at below-resonant energies.

energies and ordering is beyond the scope of the present Letter; nevertheless, the model emphasizes that there are different possible polarization mechanisms. When pumping at the photoconductivity threshold or below (<830 nm [23]), additional mechanisms are expected to occur: further work is required to understand the electronic structure and spin polarization mechanism of SiV^0.

Bulk spin polarization and long spin lifetimes at 30 K and below, combined with a high Debye-Waller factor and infrared emission, establish SiV^0 as a defect which demands further study. In particular, optical stress measurements would unambiguously identify the excited state of the 946 nm ZPL and, in turn, aid in the interpretation of the observed echo-detected 134 GHz ZPL splitting. Additionally, demonstration of spin-dependent photoluminescence contrast would enable the rapid determination of center properties and enable its exploitation as, e.g., a remote temperature sensor. The ability to efficiently spin-polarize SiV^0 at wavelengths which do not affect NV^- opens the possibility of protocols which use NV^- as a control or readout mechanism, but where multiple proximal qubits can be initialized independently of the NV^- center and within the same optically addressed volume. The 946 nm wavelength falls within the 980 nm band, where down-conversion to the telecoms 1550 nm wavelength has already been demonstrated [37], and this motivates further study to investigate possible exploitation of this defect in quantum communication applications.

We thank TOPTICA Photonics AG for the use of the CTL 950 tuneable laser, and Adam Gali and Gergö Thiering for useful discussion. This work was supported by EPSRC Grants No. EP/J500045/1 and No. EP/M013243/1.

*Corresponding Author.
b.green@warwick.ac.uk
†m.e.newton@warwick.ac.uk

[1] M. W. Doherty, N. B. Manson, P. Delaney, F. Jelezko, J. Wrachtrup, and L. C. L. Hollenberg, Phys. Rep. **528**, 1 (2013).
[2] L. Rondin, J.-P. Tetienne, T. Hingant, J.-F. Roch, P. Maletinsky, and V. Jacques, Rep. Prog. Phys. **77**, 056503 (2014).
[3] P. Maletinsky, S. Hong, M. S. Grinolds, B. Hausmann, M. D. Lukin, R. L. Walsworth, M. Loncar, and A. Yacoby, Nat. Nanotechnol. **7**, 320 (2012).
[4] A. Faraon, C. Santori, Z. Huang, V. M. Acosta, and R. G. Beausoleil, Phys. Rev. Lett. **109**, 033604 (2012).
[5] E. Neu, D. Steinmetz, J. Riedrich-Möller, S. Gsell, M. Fischer, M. Schreck, and C. Becher, New J. Phys. **13**, 025012 (2011).
[6] J. N. Becker, J. Görlitz, C. Arend, M. L. Markham, and C. Becher, Nat. Commun. **7**, 13512 (2016).
[7] B. Pingault, D.-D. Jarausch, C. Hepp, L. Klintberg, J. N. Becker, M. Markham, C. Becher, and M. Atatüre, Nat. Commun. **8**, 15579 (2017).
[8] K. Iakoubovskii and A. Stesmans, Phys. Status Solidi A **186**, 199 (2001).
[9] A. M. Edmonds, M. E. Newton, P. M. Martineau, D. J. Twitchen, and S. D. Williams, Phys. Rev. B **77**, 245205 (2008).
[10] U. F. S. D'Haenens-Johansson, A. M. Edmonds, B. L. Green, M. E. Newton, G. Davies, P. M. Martineau, R. U. A. Khan, and D. J. Twitchen, Phys. Rev. B **84**, 245208 (2011).
[11] A. Gali and J. R. Maze, Phys. Rev. B **88**, 235205 (2013).
[12] V. M. Acosta, E. Bauch, M. P. Ledbetter, A. Waxman, L. S. Bouchard, and D. Budker, Phys. Rev. Lett. **104**, 070801 (2010).
[13] A. M. Edmonds, U. F. S. D'Haenens-Johansson, R. J. Cruddace, M. E. Newton, K.-M. C. Fu, C. Santori, R. G. Beausoleil, D. J. Twitchen, and M. L. Markham, Phys. Rev. B **86**, 035201 (2012).
[14] M. Lesik, J.-P. Tetienne, A. Tallaire, J. Achard, V. Mille, A. Gicquel, J.-F. Roch, and V. Jacques, Appl. Phys. Lett. **104**, 113107 (2014).
[15] L. J. Rogers, K. D. Jahnke, M. W. Doherty, A. Dietrich, L. P. McGuinness, C. Müller, T. Teraji, H. Sumiya, J. Isoya, N. B. Manson, and F. Jelezko, Phys. Rev. B **89** (2014).
[16] J. P. Goss, R. Jones, S. J. Breuer, P. R. Briddon, and S. Öberg, Phys. Rev. Lett. **77**, 3041 (1996).
[17] See Supplemental Material at http://link.aps.org/supplemental/10.1103/PhysRevLett.119.096402 for details on sample preparation, spin polarization efficiency calculation, linewidth broadening at high temperature, raw polarized spectra for different excitation wavelengths, and notes on orientational sensitivity in echo-detected frequency-swept measurement, which includes Refs. [18–22].
[18] K. M. Itoh and H. Watanabe, MRS Commun. **4**, 143 (2014).
[19] L. J. Rogers, K. D. Jahnke, T. Teraji, L. Marseglia, C. Müller, B. Naydenov, H. Schauffert, C. Kranz, J. Isoya, L. P. McGuinness, and F. Jelezko, Nat. Commun. **5**, 4739 (2014).
[20] V. M. Acosta, E. Bauch, M. P. Ledbetter, C. Santori, K.-M. C. Fu, P. E. Barclay, R. G. Beausoleil, H. Linget, J. F. Roch, F. Treussart, S. Chemerisov, W. Gawlik, and D. Budker, Phys. Rev. B **80**, 115202 (2009).
[21] H. Pinto, R. Jones, D. W. Palmer, J. P. Goss, P. R. Briddon, and S. Öberg, Phys. Status Solidi B **209**, 1765 (2012).
[22] H. Clevenson, M. E. Trusheim, C. Teale, T. Schröder, D. Braje, and D. Englund, Nat. Phys. **11**, 393 (2015).
[23] L. Allers and A. T. Collins, J. Appl. Phys. **77**, 3879 (1995).
[24] K. Mohammed, G. Davies, and A. T. Collins, J. Phys. C **15**, 2779 (1982).
[25] C. Hepp, T. Müller, V. Waselowski, J. N. Becker, B. Pingault, H. Sternschulte, D. Steinmüller-Nethl, A. Gali, J. R. Maze, M. Atatüre, and C. Becher, Phys. Rev. Lett. **112**, 036405 (2014).
[26] T. Müller, C. Hepp, B. Pingault, E. Neu, S. Gsell, M. Schreck, H. Sternschulte, D. Steinmüller-Nethl, C. Becher, and M. Atatüre, Nat. Commun. **5**, 3328 (2014).
[27] A. Jarmola, V. M. Acosta, K. Jensen, S. Chemerisov, and D. Budker, Phys. Rev. Lett. **108**, 197601 (2012).
[28] C. Slichter, *Principles of Magnetic Resonance*, 3rd ed. (Springer-Verlag, Berlin, 1990).
[29] A. Abragam and B. Bleaney, *Electron Paramagnetic Resonance of Transition Ions*, 2nd ed. (Dover Publications, Inc., New York, 1986).

[30] A. Schweiger and G. Jeschke, *Principles of Pulse Electron Paramagnetic Resonance Spectroscopy* (Oxford University Press, Oxford, 2001).

[31] F. Dolde, I. Jakobi, B. Naydenov, N. Zhao, S. Pezzagna, C. Trautmann, J. Meijer, P. Neumann, F. Jelezko, and J. Wrachtrup, Nat. Phys. **9**, 139 (2013).

[32] S. Zaiser, T. Rendler, I. Jakobi, T. Wolf, S.-Y. Lee, S. Wagner, V. Bergholm, T. Schulte-Herbrüggen, P. Neumann, and J. Wrachtrup, Nat. Commun. **7**, 12279 (2016).

[33] P. L. Stanwix, L. M. Pham, J. R. Maze, D. Le Sage, T. K. Yeung, P. Cappellaro, P. R. Hemmer, A. Yacoby, M. D. Lukin, and R. L. Walsworth, Phys. Rev. B **82**, 201201 (2010).

[34] M. W. Doherty, N. B. Manson, P. Delaney, and L. C. L. Hollenberg, New J. Phys. **13**, 025019 (2011).

[35] M. L. Goldman, M. W. Doherty, A. Sipahigil, N. Y. Yao, S. D. Bennett, N. B. Manson, A. Kubanek, and M. D. Lukin, Phys. Rev. B **91**, 165201 (2015).

[36] V. Ivády, K. Szász, A. L. Falk, P. V. Klimov, D. J. Christle, E. Janzén, I. A. Abrikosov, D. D. Awschalom, and A. Gali, Phys. Rev. B **92**, 115206 (2015).

[37] Q. Li, M. Davanco, and K. Srinivasan, Nat. Photonics **10**, 406 (2015).